

## Present-day heat flow, thermal history and tectonic subsidence of the East China Sea Basin

Shuchun Yang<sup>a,\*</sup>, Shengbiao Hu<sup>a</sup>, Dongsheng Cai<sup>b</sup>, Xiaojie Feng<sup>b</sup>, Linlin Chen<sup>c</sup>, Le Gao<sup>b</sup>

<sup>a</sup>*Institute of Geology and Geophysics, Chinese Academy of Sciences, Beijing 100029, People's Republic of China*

<sup>b</sup>*China Offshore Oil Exploration and Development Research Center, Hebei 074010, People's Republic of China*

<sup>c</sup>*Bureau of Marine Geology of Shanghai MGRC, Shanghai, People's Republic of China*

Received 17 September 2003; received in revised form 17 May 2004; accepted 20 May 2004

### Abstract

The East China Sea Basin is located in the convergence area between the Eurasian plate, the Pacific plate and the Philippine Sea plate, and consists of two depressions, the Taibei Depression in the west and the Xihu Depression in the east. Heat flow measurements show that the East China Sea Basin is characterized by present-day heat flow around 70.6 mW/m<sup>2</sup>, varying between 55 and 88 mW/m<sup>2</sup>. No significant difference in heat flow is observed between the Xihu and the Taibei Depressions. Thermal history reconstruction using vitrinite reflectance suggests that the thermal history was, however, different in the Taibei and the Xihu Depressions. Paleo-heat flow values when the pre-Tertiary formations experienced their maximum temperature at the end of the Paleocene reached a mean of 82 mW/m<sup>2</sup> in the Taibei Depression, much higher than the present-day value. The lower Tertiary sediments in the Xihu Depression experienced maximum temperatures at the end of Oligocene (35.4–23.3 Ma) and reached a mean paleo-heat flow value of 83 mW/m<sup>2</sup>. Tectonic subsidence analysis shows that the timing of the major rifting episode was different across the East China Sea Basin. The rifting occurred from the Late Cretaceous (~65 Ma) to the early Eocene (~55 Ma) in the Taibei Depression, followed by thermal subsidence from the late Eocene to the end of Miocene (23.3–5.2 Ma). In contrast, in the Xihu Depression the initial subsidence lasted until the early Miocene and thermal subsidence to the end of Miocene. From Pliocene to the present, an accelerated subsidence took place all along the West Pacific margin of Asia. Significant thicknesses of strata were removed from the unconformities in the basin: the mean amount of erosion was 1147 m from the Paleocene and 1208 m above the Oligocene in the Taibei Depression, and 1409 m from the Oligocene in the Xihu Depression.

© 2004 Elsevier Ltd. All rights reserved.

*Keywords:* East China Sea basin; Heat flow; Thermal history; Tectonic subsidence; Thermo-tectonic evolution

### 1. Introduction

Many extensional basins, which contain significant petroleum resources, developed in eastern China after the late Mesozoic. These basins, both onshore and offshore, have a similar age and structural style. The sedimentation and structural geometry of these basins have been described in several earlier publications (e.g. Gilder, Keller, Luo, & Goodell, 1991; Li, 1984; Li, Mo, & Yang, 1995; Li, Yang, & Wu, 1987; Li, Yang, & Xie, 1997; Ma & Wu, 1987; Tian, Han, & Xu, 1992). The basins experienced episodic rifting

stages, including late Mesozoic rifting, early Tertiary rifting, Neogene rifting and Quaternary rapid subsidence. The late Mesozoic rifting was caused mainly by the westward, subduction induced slab roll-back of the Pacific plate relative to the eastern margin of Asia (Cong, 1977; Tao, 1992). Early Tertiary rifting is grouped into two systems, continental rifting and a continental margin rifting, which might be caused by the steepening dip of the subducted oceanic slab (Pigott & Ru, 1994; Ru & Pigott, 1986). Oligo-Miocene, rifting formed pull-apart basins related to regional sinistral transform faulting, while a later phase of rifting was caused by E–W extension since the Pliocene (Kimura & Tamaki, 1986; Tapponnier & Molnar, 1979). Rapid, regional Quaternary subsidence has been observed all along the West Pacific margin of Asia.

\* Corresponding author.

E-mail addresses: ysc740316@mail.igcas.ac.cn (S. Yang), sbhu@mail.igcas.ac.cn (S. Hu).

Its origin remains unclear though [Zhong et al. \(2001\)](#) have related this rapid subsidence to the dramatic uplift of the Tibetan Plateau.

Reconstruction of the thermal history of the East China Sea Basins is critical to our understanding of the geodynamics of post-Mesozoic extension, and hence to our ability to accurately assess the petroleum potential of these basins. A lack of detailed geothermal data from the basins, especially from the offshore basins, has considerably weakened the discussion of the rift dynamics. In recent years, the discovery of several new oil fields by Chinese and foreign oil companies has inspired comprehensive studies on the origin and tectonic evolution of the offshore basins. Data including borehole temperature logs and thermal organic maturity measurements have accumulated quickly. To provide a more complete database for addressing the thermal regime

and related rifting process, we have studied the present-day temperature profiles and vitrinite reflectance data, and attempted to reconstruct the thermal and tectonic subsidence history, and based on these data, discussed the thermo-tectonic evolution of the East China Sea Basin.

### 2. Geological setting

The East China Sea lies in the convergence zone between the EurAsiaN plate, the Pacific plate and the Philippine Sea plate. This zone consists of, from west to east, the Min-Zhe Uplift belt, the East China Sea Basin, the Diaoyudao Folded Uplift belt, the frontal basin of continental shelf, the Okinawa Trough, the Ryukyu Arc and Ryukyu Trench ([Fig. 1](#)). The Diaoyudao Folded Uplift belt is often referred

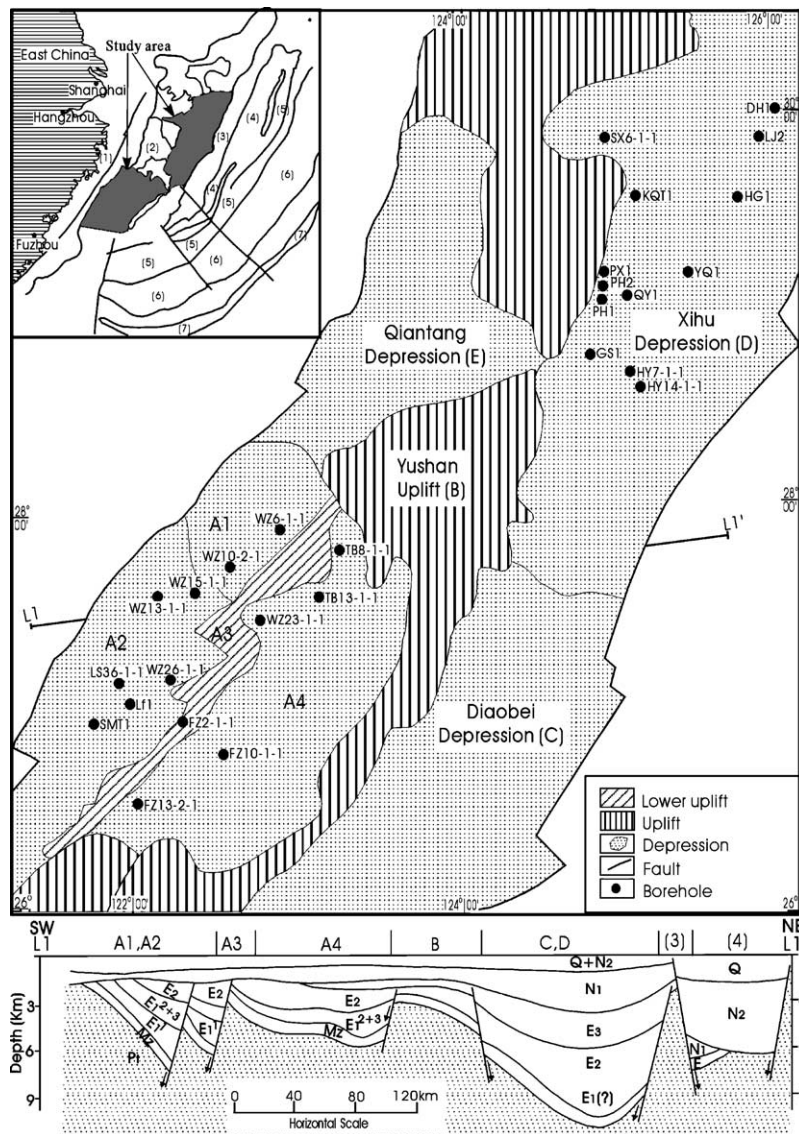


Fig. 1. General structure of the East China Sea basin and the cross section (L1–L1'). Inset map shows the locality of the basin and the tectonic units: (1) Min-Zhe Uplift belt; (2) East China Sea basin; (3) Diaoyudao Folded Uplift belt; (4) The frontal basin of continental shelf; (5) Okinawa Trough; (6) Ryukyu Island and (7) Ryukyu Trench.

Table 1  
Summary of the East China Sea basin stratigraphy

Era	System	Series	Formation	Age (Ma)	Code	Tectonic events	Thickness (m)
Cenozoic	Quaternary		Donghai	1.64	Q	Taiwan movement	250–400
		Tertiary					
		Pliocene	Santan	5.2	N2		200–500
		Miocene	Liulang	10.4	N1ll		100–200
	Yuquan		16.3	N1yq		100–200	
			Longjing	23.3	N1lj	Longjing movement	0–300
		Oligocene	Huagang	35.4	E3hg		
		Eocene	Pinghu	38.6	E2ph	Yuquan movement	
	Wenzhou		50	E2wz		300–600	
	Oujiang		56.5	E2oj	Oujiang movement	200–800	
		Paleocene	Mingyuefeng	57.8	E1myf		100–500
	Lingfeng		60.5	E1lf		200–1000	
	Yueguifeng		65	E1ygf	Yandang movement	2000–3000	
Mesozoic	Cretaceous	Up	Shimentan	96	K <sub>2smt</sub>		175
			Mingjiang		K <sub>2mj</sub>		372.5
			Yushan		K <sub>2ysh</sub>		397.5
		Lower	Xiamen	135	K <sub>1xm</sub>		540
	Jurassic		Mid-Lower	Fuzhou	203	J <sub>1-J2</sub>	

to as the Diaoyudao Island Uplift or the Taiwan-Sinzi Folded Zone (Wageman, Hilde, & Emery, 1970). The East China Sea Basin, as a part of the East China Sea continental shelf, consists of the Taibei and Xihu Depressions (see Fig. 1). Regional structures strike roughly NE and the basin is filled with water ~100 m deep. The Taibei Depression is divided into four parts, (1) the Jiaojiang Sag, (2) Lishui Sag, (3) Fuzhou Sag, and (4) the Yandang lower-uplift. The Okinawa Trough, which abuts the Xihu Depression, is an active rift basin related to the subduction of Philippine Sea plate under the Eurasian plate (Kimura, 1985).

The basement of the East China Sea Basin is metamorphic rock of Proterozoic age, sampled in boreholes WZ6-1-1 and LF1 in the Lishui and the Jiaojiang Sags (Qiu & Gong, 1999). The metamorphic basement is covered predominantly by mudstone and sandstone formations of Jurassic to Quaternary age. Mesozoic volcanic rocks are observed only locally in the Taibei Depression. Tertiary strata are typically sandstone and mudstone, with minor coal and limestone. Quaternary sequences consist mainly of clay and mudstone (Table 1).

Five periods of tectonic activity have been recognized within the basin. The first, the Yandang movement (~65 Ma), began in the late Cretaceous, which resulted in the rifting of the basin and formation of a half-graben striking NNE-NE (Fig. 1). The second, the Oujiang movement, began at the end of Paleocene (~57 Ma) and was characterized by uplift and erosion of the base of the half-graben. The third, Yuquan movement began at the end of Eocene (~36 Ma), the fourth, the Longjing movement, began at the end of the late Miocene (~10 Ma), while the fifth, the Taiwan movement began in the Pliocene (~5 Ma) (see Table 1).

A number of tectonic models had been proposed for the formation of the East China Sea basin, including, (1) simple shear (Yu & Chow, 1997); (2) back-arc extension

(Wang, 1987); (3) two episodes of extension (Teng, 1992); and (4) extension in the presence of a hot spot (Sun & Hsu, 1991). Despite the different conclusions of these models, they each relate the evolution of the basin to the subduction of the Pacific plate.

### 3. Present-day temperature and heat flow

Downhole temperature data from the East China Sea Basin have been collected. These data include corrected bottom hole temperature (BHT) or the oil-fluid temperature (OFT) data from 24 wells and a continuous temperature log in Well Donghai-1 (DH1) (Fig. 2). From these data, including those from Xu, Jiao, Yue, and Wei (1995) for the Xihu Depression, it is seen that temperature gradients in the East China Sea Basin vary from 25 to 43 °C/km, with a mean of 32.7 °C/km (Table 2).

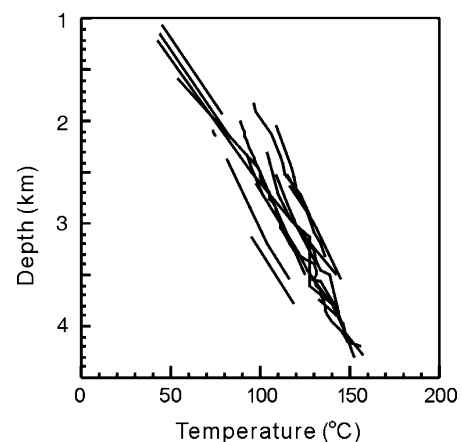


Fig. 2. Borehole temperature variations with depth in the East China Sea Basin.

Table 2  
Heat flow values and related parameters in the East China Sea Basin

Well	Longitude (E)	Latitude (N)	Depth range (m)	G (°C/km)	K (W/mK)	Heat flow (mW/m <sup>2</sup> )
FZ13-2-1	122°1.7'	26°32.6'	1200–3500	43.5	1.87	81
FZ10-1-1	122°23.2'	26°47.85'	1578–3500	37.7	1.92	72
LS36-1-2	121°53.45'	27°7.95'	2249–2723	37.2	1.83	68
WZ15-1-1	122°22.04'	27°35.96'	1053–1926	38.1	1.87	71
WZ13-1-1	122°7.88'	27°34.89'	3340–3653	31.5	2.13	67
WZ10-2-1	122°35.3'	27°43.77'	1140–2166	38.2	1.91	73
HY14-1-1	125°10.35'	28°38.2'	2515.5–3544	29.8	2.24	67
PX1	124°56.34'	29°12.35'	0–2775.7	27.2	2.20	61
QY1	125°5.04'	29°5.35'	3738.3–4284.2	30.1	2.32	70
YQ1	125°24.9'	29°5.8'	1818.9–2913.6	29.5	2.27	67
KQT1	125°8.67'	29°35.1'	3546–4303.9	27.1	3.13	85
LJ2	125°56.1'	29°52.75'	2974–4060	37.2	2.19	81
SX6-1-1	124°47.55'	29°54.2'	0–1635	25	2.20	55
WZ26-1-1	122°13.2'	27°10.1'	0–2361	29.0	2.35	68
WZ6-1-1	122°53.7'	27°55.45'	2360–3237.7	29.3	2.03	59
DH1	126°2.72'	30°1.14'	2000–4200	28.5	2.40	68
SMT1	121°44.94'	26°56.3'	109–3340	30.8	2.30	71
MYF1	122°15.8'	27°27.9'	110–2970	32.1	2.20	71
MRF1	124°35.55'	31°39.78'	3262–3535	25.6	2.19	56
PH2 <sup>a</sup>	124°55.90'	29°8.2'	2517–3506.8	29.7	2.42	72
PH1 <sup>a</sup>	124°35.21'	29°4.13'	2712–2970	31.1	2.03	63
HY7-1-1 <sup>a</sup>	125°6.3'	28°42.8'	2808.6–2987	31.1	2.24	70
TWT1 <sup>a</sup>	125°0.2'	28°32.1'	2661.5–3389.5	28.3	2.34	66
HG1 <sup>a</sup>	125°47.54'	29°34.32'	3132.6–3148.3	28.4	3.12	87
GS1 <sup>a</sup>	124°55.90'	28°45.9'	2808–3381.3	33.1	2.63	88
JS1 <sup>a</sup>	125°46.82'	30°17.94'	2400–3600	32.8	2.30	76

<sup>a</sup> Data from Xu et al. (1995).

Forty-one core samples were collected from boreholes and determined by a rock conductivity meter using a transient ring heat source. The measured conductivity values for different lithologies are shown in Table 3. The thermal conductivity values vary between 0.96 and 3.4 W/mK, with a mean of 1.79 W/mK. Mudstone and sandstone showed low values and a wide variation and the dolomite while volcanic rocks showed higher values but a relatively narrow range, because the clastic rocks have variable mineral compositions and degrees of compaction. For the total stratigraphy, the average thermal conductivity was calculated using thickness-weighted method.

Eight previously published heat flow values vary from 56 to 88 mW/m<sup>2</sup>, with a mean of 72 mW/m<sup>2</sup> (Xu et al., 1995). The thermal gradient calculated from the BHT and OFT data ranged from 25 to 43.5 °C/km, with a mean of 32.1 °C/km. The corresponding new heat flow values varied between 55 and 85 mW/m<sup>2</sup> with a mean of 70.6 mW/m<sup>2</sup>. The heat flow values in the Taibei Depression vary from 59 to 81 mW/m<sup>2</sup>, with a mean of 70.3 mW/m<sup>2</sup>, while the heat flow values in the Xihu Depression vary between 55 and 88 mW/m<sup>2</sup> with a mean of 70.8 mW/m<sup>2</sup> (Table 2). These values suggest there is no significant difference in heat flow between the Taibei and Xihu Depressions.

The regional heat flow pattern in the East China Sea Basin suggests that the measured heat flow is controlled by

shallow factors, such as the variation in lithofacies and thermal conductivity structure, as well as heat refraction effects along faults. By way of comparison, the mean value of heat flow in the East China Sea Basin is lower than that in the South China Sea Basin, which has a mean heat flow value of 78.7 mW/m<sup>2</sup> (He, Xiong, & Wang, 1998; He, Wang, Xiong, & Wang, 2001). Furthermore, the heat flow in the East China Sea Basin is substantially higher than that expected for a typical cratonal basin, such as the Junggar Basin, which has a mean heat flow value of 45 mW/m<sup>2</sup> (Wang, He, & Wang, 2001). In the adjacent Okinawa Trough, heat flow values are much higher, measuring between 100 and 900 mW/m<sup>2</sup> (Yu & Li, 1992). These heat flow data therefore suggest that the East China Sea Basin is geothermally not a modern back-arc basin.

#### 4. Thermal history reconstruction

##### 4.1. Thermal indicator

Thermal indicator data in the East China Sea Basin consists of several hundred vitrinite reflectance (VR) measurements made at different depths from 20 boreholes. Fig. 3 shows VR values plotted vs depth in the entire depression and in representative boreholes. The VR values

Table 3  
Thermal conductivity values from 41 samples in the East China Sea Basin

Well	Depth (m)	Stratum	Lithology	Conductivity (W/mK)	Well	Depth (m)	Stratum	Lithology	Conductivity (W/mK)
FZ13-2-1	1814	K2	Sandstone	0.96	HY7-1-1	3043	E3H	M.S.	2.05
DH1	3452	E3H	F.S.	1.45		3198	E3H	M.S.	2.23
	3678	E3H	Mudstone	1.5		3611	E3H	C.S.	2.97
	4107	E3H	Sandstone	1.7		3380	E3H	Mudstone	2.3
	3416	E3H	F.S.	1.75		2814	E3H	F.S.	1.85
	3203	E3H	Mudstone	1.55		2816	E3H	F.S.	1.92
	3032	E3H	Mudstone	1.95		2987	E3H	C.S.	2.1
	2513	E3H	Sandstone	1.55		3194	E3H	Mudstone	1.55
	2514	E3H	Sandstone	1.6	WZ6-1-1	2644	E1	Sandstone	1.32
	1232	N2S	Mudstone	1.25		2882	E1	M.S.	1.83
	1232	N2S	Mudstone	1.18		2890	E1	C.S.	2.1
	3681	E3H	Sandstone	1.85		3146	E1	Mudstone	1.88
	3452	E3H	Sandstone	2		3149	E1	M.S.	1.91
HY7-1-1	1461	N11l	Mudstone	1.02		3140	E1	Conglomerate	1.75
	1955	N1y	F.S.	1.1		3547	BASE	Volcanic	3.42
	1962	N1y	M.S.	1.25		2639	J1-J2	C.S.	1.35
	1967	N1y	C.S.	1.15	FZ10-1-1	2589	K2smt	Mudstone	3
	2276	N11j	Sandstone	1.35	TB8-1-1	2581	K2smt	Sandstone	2.32
	2583	E3H	F.S.	1.5		2706	K2smt	Sandstone	2.32
	2773	E3H	M.S.	1.6		3471	T1	Limestone	2.82
	2773	E3H	F.S.	1.75					

F.S., fine-grained sandstone; M.S., medium-grained sandstone; C.S., coarse-grained sandstone.

varied between 0.2 and 1.8%. The VR data from the Taibei Depression can be divided into two groups (Fig. 3A and C); one is less than 0.7% from the Tertiary formation and has lower gradient; another ranges from 0.7 to 1.4% from the pre-Tertiary formation and has a higher gradient. In the Xihu Depression, the drilled formations are restricted to the Tertiary (Fig. 3B), however, VR values show a clear increase with depth (Fig. 3D).

#### 4.2. Method

Quantitative methods of thermal reconstruction through inversion of thermal indicators are based on kinetic models, i.e. forward models, of different thermal indicators. These methods fall into three categories: (1) stochastic inversion methods of a single sample (e.g. Lutz & Omar, 1991), (2) paleogeothermal gradient-based method of a vertical sequence of samples (Bray, Green, & Duddy, 1992; Duddy, Green, Hegarty, & Bray, 1991) and (3) heat flow based methods based on a suite of downhole samples (Lerche, Yarzab, & Kendall, 1984). Methods in the second category, which have been employed in this study considering the data situation of the thermal indicator, estimate the paleogeothermal gradient from the maximum paleo-temperature profile determined for a vertical sequence of samples from a well. In this case the thermal history is assumed to have cooled from the maximum temperature to the later time or the present-day temperatures. An advantage to this method is that it requires no reconstruction of the burial history, however, a major

disadvantage is that it does not take into account the variation of thermal conductivity both with depth (different rocks) and with time (compaction). In addition, the radiogenic heat production of rocks is treated as negligible (Hu, Paul, O'Sullivan, & Barry, 2001). In respect to the situation of both geological evolution and the VR data, the method of paleo-temperature gradient method was selected to reconstruct the thermal history in the East China Sea Basin.

In practice, the sedimentary section in any given borehole is divided into separate sequences bound by unconformities. These sequences can then be combined into subsections in which all formations experienced maximum paleo-temperature at the same time. If the maximum paleo-temperature for a given subsection occurred in the past, as opposed to the present, and, if different subsections reached the maximum temperature at different time, then this approach allows constraints derived from the shallower levels of the stratigraphy to be placed onto the thermal history of the lower or the earlier ones. This method therefore allows separation of superimposed thermal effects from multiple thermo-tectonic events. The framework of thermal indicator inversion based on temperature gradient is shown in Fig. 4.

The thickness removed from above an unconformity can be estimated as follow

$$E = (T_i - T_s)/(dT/dz) \quad (1)$$

where  $E$  is the erosion upon the unconformity in meters,  $T_i$  is the paleo-temperature at the unconformity,  $T_s$  is

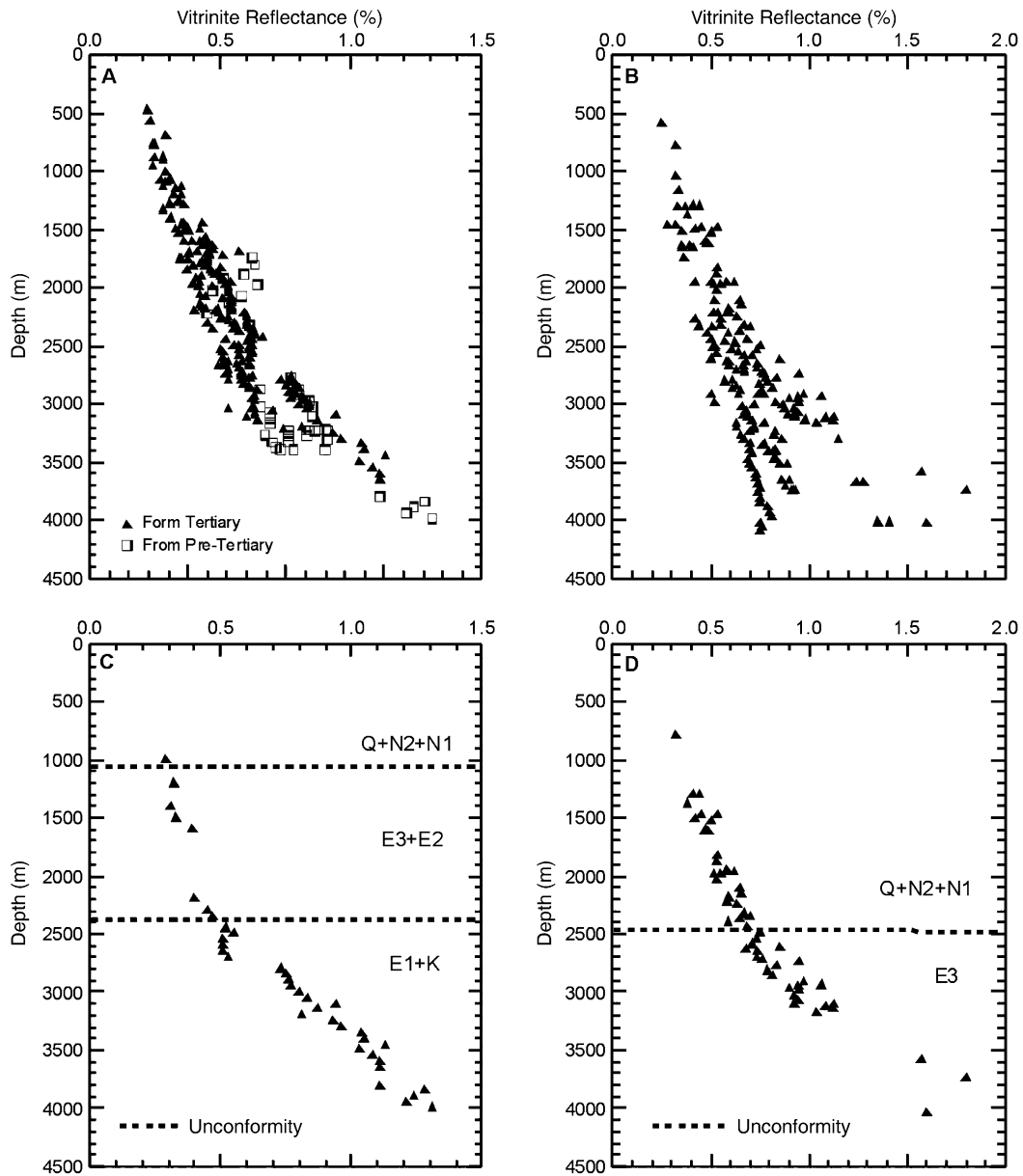


Fig. 3. Vitrinite reflectance (VR) distribution with depth for the studied wells in the East China Sea Basin. (A) VR data vs depth in the Taibei Depression; (B) VR data vs depth in the Xihu Depression; (C) VR data vs depth in Well WZ26-1-1 in the Taibei Depression and (D) VR data vs depth in Well DH1 in the Xihu Depression.

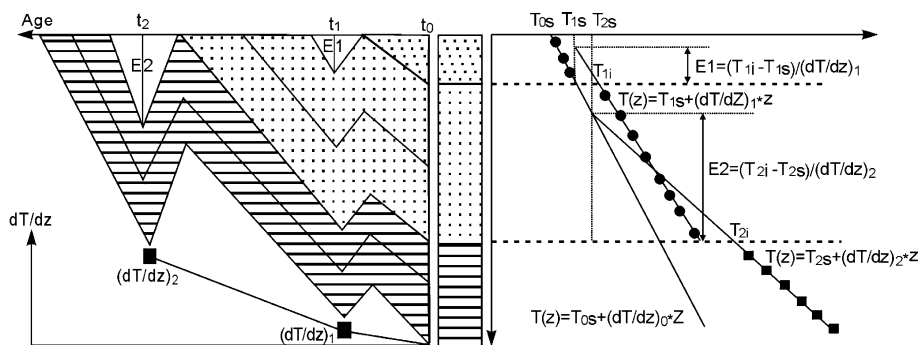


Fig. 4. The burial and thermal gradient histories (left) and the maximum paleo-temperature profiles (right) for the three subsections experienced their maximum paleotemperatures at different times, as well as the relationship between the paleo-temperature gradient( $(dT/dz)_i$ ) and the eroded thickness ( $E_i$ ).

the paleo-surface temperature and  $dT/dz$  is the maximum paleo-temperature gradient.

In fact, the temperature gradient dramatically decreases downwards in the near surface part of the section, with unconsolidated cover in the absence of groundwater disturbance. While the assumption of linear temperature distribution is valid for an ideal homogeneous medium or over a limited depth interval, this assumption does not hold for the layered sedimentary media at shallow depth in a basin with unconsolidated sedimentary cover and significant compaction of rocks.

If no groundwater disturbance is present and the effect of sedimentation and long-term climate change is ignored, steady-state heat conduction can be assumed in the sedimentary pile. The temperature distribution under the assumption of 1D, purely conductive and steady-state heat transfer, the governing equation is (Carlaw & Jaeger, 1959)

$$\frac{d}{dz} \left\{ K(z) \frac{dT(z)}{dz} \right\} + A(z) = 0. \quad (2)$$

where the temperature  $T$ , heat production  $A(z)$ , and thermal conductivity  $K(z)$  are function of the porosity ( $\phi(z)$ ) of the sediment, and  $\phi(z)$  is a function of the burial depth ( $z$ ), and taken assuming the following boundary ( $z=0$ ) conditions:

$$T(0) = T_s, \quad \left( \frac{dT}{dz} \right)_0 = \frac{q_s}{K_s} \quad (3)$$

where  $T_s$  is constant paleosurface temperature,  $q_s$  the heat flow at the surface, and  $K_s$  the average thermal conductivity of the near surface sediments. Under these boundary conditions, the 1D steady-state solutions can be given analytically by

$$T(z) = T_s + \frac{1}{K} q_s z - \frac{A}{2K} z^2 \quad (4)$$

where  $A$  varies with depth but it is assumed to be constant in a very limited depth interval (2 m for computation). In this procedure,  $K$  is automatically calculated according to the paleoporosity as  $K = K_s^{(1-\phi)} K_w^\phi$ , where  $K_s$  and  $K_w$  are thermal conductivity for the sediment matrix and the saturated water, respectively. The  $\phi(z,t)$  can be reconstructed using the ‘backstripping’ method of Sclater and Christie (1980), which assumes the matrix thickness of the rocks have no change but porosity decrease with compaction.

Fig. 5 shows the temperature profile before the section above unconformity was eroded. Clearly, the projected intercepts ( $T_s^*$ ) have significant offset from the surface temperature ( $T_s$ ), such that the greater the buried depth, the greater the offset. If the temperature distribution is described by  $T_s$  and  $(dT/dz)$  as for case A, the temperature profile will obviously be discordant with the theoretical profile (see Fig. 5). The magnitude of this discordance will depend on the compaction factor and the initial porosity of the removed formation, as well as the thickness of the removed section.

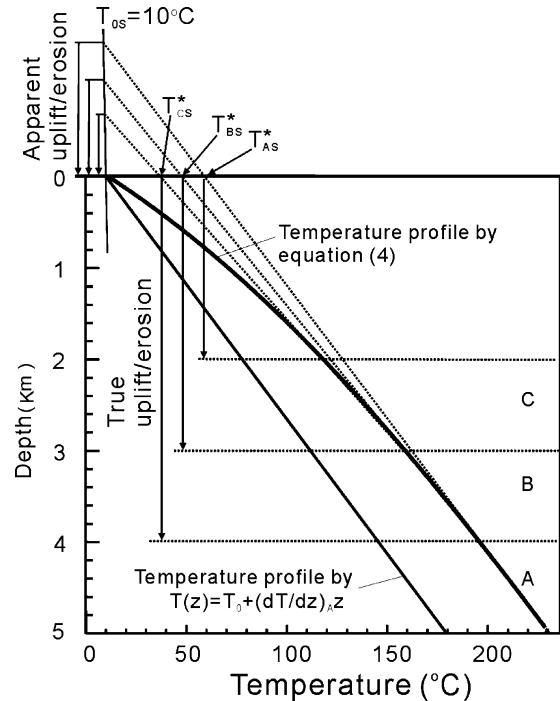


Fig. 5. Vertical temperature distribution for the sediment piles consisted of sandstone (50%) and mudstone (50%). The offset between the projection intercept ( $T_s^*$ ) and the surface temperature ( $T_s$ ) increases with buried depth of the remained section (depths A, B and C).

This means the intercept of the paleo-temperature profile ( $T_s^*$ ) in the remaining section is not the same as the paleo-surface temperature ( $T_s$ ) (see Fig. 5). Therefore, the  $T_s$  in Eq. (1) should be replaced by the intercept ( $T_s^*$ ) in order to obtain an eroded thickness, otherwise an apparent erosion will be added into the estimated thickness resulting in overestimation of the eroded thickness.

### 4.3. Results

The maximum temperature profiles as derived from VR data using the chemical kinetic model (Sweeney & Burnham, 1990) in all boreholes show that paleo-temperatures during Early Tertiary and the pre-Tertiary formations are higher than the present-day temperature, indicating that these formations experienced the maximum temperatures in the past (Table 4).

In the Taipei Depression, there are four unconformities (see Table 1), however, only two or three subsections can be recognized from the maximum paleo-temperature profiles (Table 4). The Jurassic and the Cretaceous layers are assigned to one subsection as their derived maximum paleo-temperatures are similar, and are also significantly different from the upper sections. Their similarity indicates they reached maximum paleo-temperature at the same time and, therefore that the entire Mesozoic reached maximum paleo-temperature at an earlier time, most likely during the unconformity between the late Paleocene and the early Eocene. The derived paleo-temperatures in the overlying

Table 4  
The reconstructed thermal history and eroded stratigraphic thicknesses at the unconformities in each borehole

Well	Unconformity on the Oligocene			Unconformity on the Paleocene			Unconformity on the Mesozoic		
	G (°C/km)	Heat flow (mW/m <sup>2</sup> )	E (m)	G (°C/km)	Heat flow (mW/m <sup>2</sup> )	E (m)	G (°C/km)	Heat flow (mW/m <sup>2</sup> )	E (m)
FZ10-1-1	25.0	48.1	1509				31.1	70.5	1240
FZ13-2-1							32.9	74.3	1195
WZ23-1-1	30.4	59.5	1331						
FZ2-1-1	33.0	66.8	1516						
WZ33-1-1	37.8	69.3	907						
LS36-1-1				35.8	67.0	916			
LS36-1-2				33.7	83.0	1365			
WZ26-1-1	30.0	56.5	740	48.4	94.6	1160			
WZ10-2-1	29.6	55.5	1022						
WZ6-1-1	26.6	57.5	1433						
Mean	30.3	59.0	1208	39.3	81.5	1147	32	72.4	1220
DH1	50.1	91.3	1593						
LJ2	43.7	80.5	1704						
HY14-1-1	43.1	78.5	995						
HY7-1-1	48.3	98.6	1081						
NB2-1-1	32.3	68.3	1672						
Mean	43.5	83.4	1409						

G, temperature gradient; E, the eroded thickness at the unconformity.

section from the Eocene to the Oligocene, are also higher than the present-day temperatures, indicating this section experienced maximum temperatures during the late Oligocene to the early Miocene. This time interval corresponds to the time gap for the unconformity between the late Oligocene to the early Miocene. In contrast, the surface subsection, corresponding to Miocene to present, reached the maximum temperature and burial depth at present-day. For different boreholes, the recorded paleo-temperature gradients derived from the VR data as well as the time when the subsections reached maximum temperature are different, depending on the structural location (sag or uplift) and the age of stratigraphy penetrated by the boreholes.

As an example, Fig. 6 shows the present-day temperature profile and paleo-temperature profiles for Well WZ26-1-1 (see Fig. 1 for the location). From the profiles, it is seen that the paleo-temperatures were higher than those in the present and that the maximum paleo-thermal gradients are different for different subsections. The Cretaceous to Paleocene, is characterized by a peak paleo-temperature gradient of 48.4 °C/km, while the gradient in the middle subsection, Eocene to Oligocene, is 30 °C/km. There is no VR data for the Miocene to present top subsection, which reached maximum burial depth at the present. Thus its peak temperature gradient is inferred to be the present-day gradient (29 °C/km).

Because the bottom and the middle subsections reached their maximum temperature at different times, the thickness removed on the unconformities on the top of the subsections can be estimated to be 1160 and 740 m, respectively. Two boreholes (FZ10-1-1, FZ13-2-1) show erosion above

the Mesozoic and a mean eroded thickness was 1220 m. The thicknesses eroded on the unconformities in the 10 studied boreholes are listed in Table 4.

In the Xihu Depression, just one unconformity above the Oligocene was penetrated by the drillholes. The derived paleo-temperatures below the unconformity are higher than the present-day temperatures, indicating that the Eocene to Oligocene experienced their maximum paleo-temperatures during the time gap of the unconformity from the late Oligocene to the early Miocene (~25 Ma). The section above the unconformity is presently at maximum temperature. The average temperature gradient for the five boreholes studied are 43.5 °C/km and the mean eroded thickness is 1409 m (see Table 4).

Temperature gradients may vary due to different thermal conductivity of the formations. For comparison, the paleo-heat flow values were calculated based on the reconstructed temperature gradients and the formation porosity, as well as the measured present-day thermal conductivity. Table 4 presents the paleo-heat flow values at the time of maximum paleo-temperature for each boreholes and Fig. 7 charts the average heat flow paths for both the Taibei and the Xihu Depressions. The thermal history prior to the Eocene (~50 Ma) cannot be reconstructed, however, as there are no samples from pre-Eocene strata. In the Taibei Depression, the maximum paleo-heat flow (~67–94.6 mW/m<sup>2</sup> with a mean of 81.5 mW/m<sup>2</sup>) was reached at the end of the Paleocene (~65 Ma) and then cooled to the present. Relatively, high heat flow seems to have lasted a longer time in the Xihu Depression followed by more recent cooling.

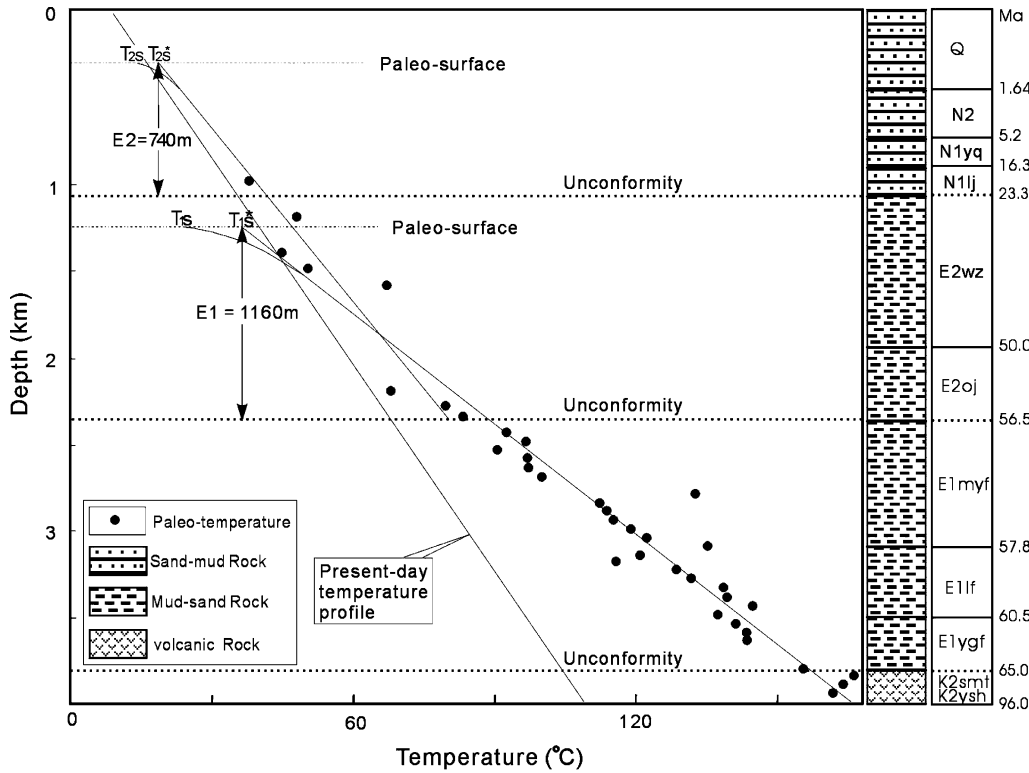


Fig. 6. The present-day and the paleo-temperature profile in Well WZ26-1-1 (see Table 1 for stratigraphic code).

### 5. Tectonic subsidence analysis

Steckler and Watts (1980) and Van Hinte (1978) have described the technique of subsidence analysis. In the present study, tectonic subsidence in the East China Sea Basin was reconstructed using a ‘standant’ method (Loup, 1993). The effect of compaction is accounted for using the Sclater and Christie (1980) method. Both boreholes and pseudo-wells from the seismic profiles have been analyzed from the Taibei Depression but just boreholes were considered in the Xihu Depression. The biostratigraphic

zonal schemes were converted to absolute age with the time scale of Chinese Geological Society (Wang & Li 1990).

The reconstructed tectonic subsidence in the East China Sea Basin is shown in Fig. 8. In the Taibei Depression, rapid initial subsidence during active extension is recognized from the late Cretaceous (~65 Ma) to the Eocene (~50 Ma). Subsequent thermal subsidence occurred from the Eocene to the Oligocene (~23.3 Ma), and then from the Miocene to the present, an accelerated subsidence occurred not just in the studied depressions but also in the entire East Asia continental margin (Hu et al., 2001; Ren, Kensaku, Li, & Zhang, 2002). The active extension in the Xihu Depression was recorded to be the end of Oligocene

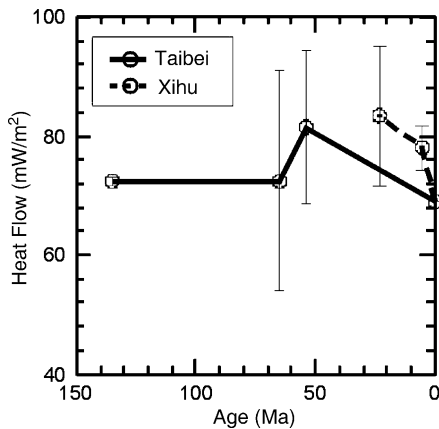


Fig. 7. The reconstructed thermal history in the East China Sea Basin. The error bars represent the range of the paleo-heat flow values for different boreholes.

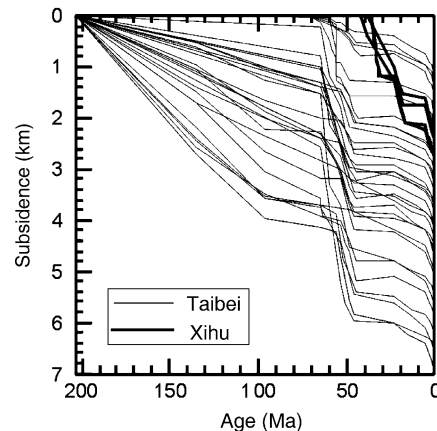


Fig. 8. Tectonic subsidence in the East China Sea Basin.

(~23 Ma) (see Fig. 8), apparently different from that of the Taibei Depression. We suggest the rifting process in the Xihu Depression ended later than that in the Taibei Depression. However, as the boreholes did not penetrate the pre-Eocene, there are no constraints on the timing of initiation of rifting in the Xihu Depression. We can, however, infer that the initial active extension in the Xihu Depression lasted until the end of the Oligocene, much longer than that in the Taibei Depression (~50 Ma). Alternatively, rifting may have started later in the Xihu Depression and if so the extension migrated eastward.

## 6. Discussion and conclusions

Based on the measurements of present-day heat flow, the thermal history reconstruction from VR data and the erosion and subsidence analysis in the East China Sea Basin, a brief discussion of the main conclusions of this paper is presented as follows:

The East China Sea Basin is characterized by present-day heat flow varying between 55 and 88 mW/m<sup>2</sup> with a mean of 70.6 mW/m<sup>2</sup>. There is no significant difference in present heat flow between the Xihu and the Taibei Depressions. The present thermal pattern shows that the East China Sea Basin is thermally and tectonically similar to the onshore areas of East China, where Cretaceous extension and magmatism were widespread (e.g. Davis et al., 1996; Faure, Sun, Shu, Monie, & Charvet, 1996; Yin & Nie, 1996). The area was also affected by eastward tectonic escape (Tapponnier, Peltzer, Le Dain, Armijo, & Cobbold, 1982) and Pacific subduction (e.g. Yin & Nie, 1996) as well as the Siberia-Mongolia-Sino-Korean collision (e.g. Enkin, Yang, Chen & Courtillot, 1992). The Cenozoic evolution of eastern Asia has been interpreted to be a result of the combined effects of the Pacific subduction and India-Eurasia collision (e.g. Molnar & Tapponnier, 1975) and that heat flow is lower than that in the South China Sea Basin (He et al., 2001).

The reconstructed thermal history suggests that the paleo-heat flow was around 82 mW/m<sup>2</sup> (~67–92 mW/m<sup>2</sup> for individual boreholes) at the end of the Paleocene (56.5 Ma), at which time the Paleocene and the pre-Tertiary sequences experienced the maximum paleo-temperature in the Taibei Depression before cooling to the present. In the Xihu Depression, the paleo-heat flow experienced by lower Tertiary strata was ~83 mW/m<sup>2</sup> (~68.3–98.6 mW/m<sup>2</sup>) at the end of the Oligocene (23.3 Ma).

Active extension in the Taibei Depression ended at ~56 Ma, followed by thermal subsidence to ~23.3 Ma, at which time active extension resumed. In contrast, in the Xihu Depression the active extension lasted until the end of Oligocene (~23.3 Ma). It is that rifting which elevated the paleoheat flow, as recorded by the VR data.

The thickness of sediment removed at the unconformities from the East China Sea Basin is inferred to have been from either the shoulder of the rifted grabens and half-grabens, or,

alternatively from regional uplifting resulted from transition from extension to compression during the tectonic evolution in the eastern Asia. In the Taibei Depression, the average eroded thickness was 1220 and 1147 m at the top of the Mesozoic and the Paleocene strata, respectively. In the Xihu Depression, the mean eroded thickness was 1409 m from the Oligocene. This removed section had a major impact on the maturation and reservation of the hydrocarbon from the pre-Tertiary source rocks.

## Acknowledgements

This research was supported by the National Science Foundation of China (NSFC) (grant No. 40172100) and a project from China National Offshore Oil Corporation. All VR data were provided by China Offshore Oil and Development Research Center and Bohai Oil Company. Shanghai Offshore Oil Company provided the core samples. This paper was greatly improved due to the careful and useful comments of an anonymous reviewer and the editor, Prof. D.G. Robert.

## References

- Bray, R. J., Green, P. F., & Duddy, I. R. (1992). Thermal history reconstruction using apatite fission track analysis and vitrinite reflectance: a case study from the East Midlands of England and the southern North Sea. In R. S. P. Hardman, *Exploration Britain: Geological insights for the next decade* (Vol. 67) (pp. 3–25). Geological Society of London Special Publication.
- Carlaw, H. S., & Jaeger, J. C. (1959). *Conduction of heat in solids*. Oxford: Oxford University Press pp. 510.
- Cong, B. (1977). Petrochemistry of Mesozoic-Cenozoic volcanic rocks in Eastern China and their geologic significance. *Chinese Science Bulletin*, 3, 245–259.
- Davis, G. A., Qian, X., Zheng, Y., Yu, H., Wang, C., Mao, T. H., et al. (1996). Mesozoic deformation and plutonism in Yunmeng Shan: a Chinese metamorphic core complex north of Beijing, China. In A. Yin, & T. M. Harrison (Eds.), *The tectonic evolution of Asia* (pp. 253–280). New York: Cambridge University Press.
- Duddy, I. R., Green, P. F., Hegarty, K. A., & Bray, R. J. (1991). Reconstruction of thermal history in basin modelling using apatite fission track analysis: what is really possible? *Offshore Australia Conference Proceedings*, 1, III49–61.
- Enkin, R. J., Yang, Z., Chen, Y., & Courtillot, V. (1992). Paleomagnetic constraints on the geodynamic history of major blocks of China from Permian to present. *Journal of Geophysical Research*, 97, 13953–13989.
- Faure, M., Sun, Y., Shu, L., Monie, P., & Charvet, J. (1996). Extensional tectonics within a subduction-type orogen: the case study of the Wugongshan dome (Jiangxi Province, southeastern China). *Tectonophysics*, 263, 77–106.
- Gilder, S. A., Keller, G. R., Luo, M., & Goodell, P. C. (1991). Timing and spatial distribution of rifting in China. *Tectonophysics*, 197, 25–243.
- He, L. J., Wang, K. L., Xiong, L. P., & Wang, J. Y. (2001). Heat flow and thermal history of the South China Sea. *Physics of the Earth and Planetary Interiors*, 126, 211–220.
- He, L. J., Xiong, L. P., & Wang, J. Y. (1998). Geothermal characteristics of the South China Sea. *China Offshore Oil and Gas*, 2, 87–90.

- Hu, S. B., Paul, B., O'Sullivan, A. R., & Barry, P. K. (2001). Thermal history and tectonic subsidence of the Bohai Basin, northern China: a Cenozoic rifted and local pull-apart basin. *Physics of the Earth and Planetary Interiors*, 126, 221–235.
- Kimura, M. (1985). Back-arc rifting in Okinawa Trough. *Marine Petroleum Geology*, 2, 222–240.
- Kimura, G., & Tamaki, K. (1986). Collision, rotation and backarc spreading: the case of the Okhotsk and Japan Sea. *Tectonics*, 5, 389–401.
- Lerche, I., Yarzab, R. F., & Kendall, C. G. St. C. (1984). Determination of paleo-heat flux from vitrinite reflectance data. *American Association of Petroleum Geologists Bulletin*, 68, 1704–1717.
- Li, D. S. (1984). Geologic evolution of petroliferous basins on continental shelf of China. *American Association of Petroleum Geologists Bulletin*, 68, 993–1003.
- Li, S., Mo, X., & Yang, S. (1995). Evolution of Circum-Pacific Basins and Volcanic belts in East China and their geodynamic background. *Earth Sciences*, 6(1), 48–58.
- Li, S., Yang, S., & Wu, C. (1987). Late Mesozoic rifting in northeast China and Northeast Asia fault basin system. *Science in China, Ser. B2*, 185–195.
- Li, S., Yang, S., & Xie, X. (1997). Tectonic evolution of tertiary basins in Circum-Pacific belt of China and their geodynamic setting. *Earth Sciences*, 8(1), 4–10.
- Loup, B. (1993). Sea-changes and extensional tectonics in the Lower Jurassic of the northern Helvetic realm (western Switzerland). In L. E. Frostyck, & R. J. Steel, *Tectonic controls and signatures in sedimentary basins. International Assessment in Sedimentology, special publication* (20).
- Lutz, T. M., & Omar, G. (1991). Inverse methods of modeling thermal histories from apatite fission track data. *Earth Planet Scientific Letters*, 104, 181–195.
- Ma, X., & Wu, D. (1987). Cenozoic extensional tectonic in China. *Tectonophysics*, 133, 243–255.
- Molnar, P., & Tapponnier, P. (1975). Cenozoic tectonics of Asia: the effects of a continental collision. *Science*, 189, 419–426.
- Pigott, J. D., & Ru, K. (1994). Basin superposition on the northern margin of South China Sea. *Tectonophysics*, 235, 27–50.
- Qiu, Z. J., & Gong, Z. S. (1999). *Petroleum exploration in China*, Vol. 4. Beijing: Petroleum Industry Publishing House pp. 911–962.
- Ren, J. Y., Kensaku, T., Li, S. T., & Zhang, J. X. (2002). Late Mesozoic and Cenozoic rifting and its dynamic setting in Eastern China and adjacent areas. *Tectonophysics*, 344, 175–205.
- Ru, K., & Pigott, J. D. (1986). Episodic rifting and subsidence in the South China Sea. *American Association of Petroleum Geologists Bulletin*, 70, 1136–1155.
- Sclater, J. G., & Christie, P. A. F. (1980). Continental stretching: an explanation of the post-mid-cretaceous subsidence of the Central North Sea Basin. *Journal of Geophysical Research*, 85, 3711–3739.
- Steckler, M. S., & Watts, A. B. (1980). The Gulf of Lion: subsidence of a young continental margin. *Nature*, 287, 425–429.
- Sun, S. C., & Hsu, Y. Y. (1991). Overview of the Cenozoic geology and tectonic development of offshore and onshore Taiwan. *TAICRUST Proceedings* (3).
- Sweeney, J. J., & Burnham, A. K. (1990). Evaluation of simple model of vitrinite reflectance based on chemical kinetics. *American Association of Petroleum Geologists Bulletin*, 10, 559–1570.
- Tao, K. (1992). *Discussion on the uniquenesses of tectono magmatism in the circum-Pacific continental margin of southeastern China. Selected Papers on Volcanic Geology and Mineral Resources of Chinese Southeast*. Beijing: Geological Publishing House pp. 1–13.
- Tapponnier, P., & Molnar, P. (1979). Active faulting and Cenozoic tectonics of the Tianshan, Mongolia, and Baikal regions. *Journal of Geophysical Research*, 84, 3425–3459.
- Tapponnier, P., Peltzer, G., Le Dain, A. Y., Armijo, R., & Cobbold, P. (1982). Propagating extrusion tectonics in Asia. *Geology*, 10, 611–616.
- Teng, L. S. (1992). Geotectonic evolution of Tertiary continental margin basins of Taiwan. *Petroleum Geology of Taiwan*, 27, 1–19.
- Tian, Z. Y., Han, P., & Xu, K. D. (1992). The Mesozoic–Cenozoic East China rift system. *Tectonophysics*, 208, 341–363.
- Van Hinte, J. E. (1978). Geohistory analysis: application of micropaleontology in exploration geology. *American Association of Petroleum Geologists Bulletin*, 62, 201–222.
- Wageman, J. M., Hilde, T. W. C., & Emery, K. O. (1970). Structural framework of East China Sea and Yellow Sea. *American Association of Petroleum Geologists Bulletin*, 54, 1611–1643.
- Wang, G. C. (1987). Formation and evolution of the East China Sea basin. *Acta Petroleum Sinica*, 8(4), 18–25.
- Wang, S., He, L. J., & Wang, J. Y. (2001). Thermal regime and petroleum systems in Junggar basin, northwest China. *Physics of the Earth and Planetary Interiors*, 126, 237–248.
- Wang, H. Z., & Li, G. C. (1990). *Correlation table of stratigraphical subdivision*. Geology Publication. Geology Press pp. 121.
- Xu, W. L., Jiao, R. C., Yue, J. Y., & Wei, D. W. (1995). Geothermal study on the continent shelf of the East China Sea. *Progresses in Geophysics*, 10, 32–38 (in Chinese).
- Yin, A., & Nie, S. (1996). A Phanerozoic palinspastic reconstruction of China and its neighboring regions. In A. Yin, & T. M. Harrison (Eds.), *The tectonic evolution of Asia* (pp. 442–485). New York: Cambridge University.
- Yu, H. S., & Chow, J. (1997). Cenozoic basins in northern Taiwan and tectonic implications for the development of the eastern Asian continental margin. *Paleogeography, Paleoclimatology, Paleocology*, 131, 133–144.
- Yu, P. Z., & Li, N. S. (1992). *Crustal heat flow of the East China Sea*. Ocean Publishing House pp. 50–74.
- Zhong, D., Ding, L., Ji, J., Zhang, J., Liu, F., Liu, J., et al. (2001). Coupling of the lithospheric convergence of west China and dispersion of East China in Cenozoic: Link with paleoenvironmental changes. *Quaternary Sciences*, 21, 303–312 (in Chinese with English abstract).